Full paper

Triboelectric nanogenerator by integrating a cam and a movable frame for ambient mechanical energy harvesting

Tinghai Cheng[a,b,c,1], Yikang Li[a,1], Yi-Cheng Wang[b,1], Qi Gao[a], Teng Ma[a], Zhong Lin Wang[b,c,*]

[a] School of Mechatronic Engineering, Changchun University of Technology, Changchun, Jilin, 130012, China
[b] School of Materials Science and Engineering, Georgia Institute of Technology, Atlanta, GA, 30332-0245, United States
[c] Beijing Institute of Nanoenergy and Nanosystems, Chinese Academy of Sciences, Beijing, 100083, China

ARTICLE INFO

ABSTRACT

Transform rotary motion triggered by environmental mechanical energy (e.g., wind) to electrical energy is widely used for energy harvesting. Triboelectric nanogenerators that are used to harvest rotational mechanical energy are mostly based on in-plane sliding or free-standing mode. However, the relative friction between the two contacting triboelectric layers may cause severe abrasion, which reduces the durability of the device and increases the maintenance cost. In this study, we report a combination of a cam and a movable frame for a novel triboelectric nanogenerator (CMF-TENG), which is expected to reduce the abrasion problem and improve the output performance. The cam is designed to transform the rotational motion triggered by ambient mechanical energy to linear movement of the movable frame, leading to a contact-separation of the triboelectric layers within each sub-triboelectrification unit of CMF-TENG, thus electric output can be generated. The average electric output from one subunit of the CMF-TENG achieved around 200 V of open-circuit voltage, 2.9 μA of short-circuit current, and 96 nC of transferred charge at the triggered rotational speed of 60 rpm. The power output increase from 180 μW (1 subunit) to around 728 μW when three subunits were connected in parallel. The output voltage of the CMF-TENG remained almost consistent throughout the roughly 8 h continuously operation, suggesting outstanding robustness and durability of the CMF-TENG. The CMF-TENG harvest energy from wind can light up 113 blue LEDs connected in series at a wind speed of 13.9 m/s with the assistance of a rectifying circuit; and can power a thermometer at the same wind speed condition with the assistance of a rectifying circuit and a capacitor. The results imply that the CMF-TENG can not only be used to harvest energy from the ambient environment, but also can achieve self-powered sensing. Technically, by using this novel design, additional sub-triboelectrification units can be added to improve the electric output of the entire device and the rotational mechanical energy can be harvested more effectively with less abrasion.

1. Introduction

Owing to the rapid growth of world energy consumption, considering the diminishing amount of non-renewable energy sources (e.g., fossil fuels), renewable and sustainable energy technology has emerged as an important field of research [1,2]. One of the most promising alternatives is to take advantage of the mechanical energy from the ambient environment. With its abundance, the omnipresent ambient mechanical energy may be used to supply the needs of energy. Therefore, several approaches, such as piezoelectric or electromagnetic, were developed to achieve this goal [3,4].

In conjunction with contact-electrification and electrostatic induction, the innovative triboelectric nanogenerator (TENG) was proposed

recently and has been developed as one of the most promising alternatives for harvesting mechanical energy [5–9]. The fundamental physics of TENG was found related to Maxwell's displacement current [10]. Compared to other approaches of energy harvesting, the TENG has raised interest worldwide in the past several years because of its lightweight, cost-effective, and abundant choice of material [11–13]. More importantly, it has been proved that TENGs can convert mechanical energy into electrical output more efficiently than widely used electromagnetic generator at lower frequencies (e.g., < 5 Hz), implying that TENG may be a great alternative for harvesting ambient mechanical energy [14].

TENG for harvesting mechanical energy is mostly based on in-plane sliding [15–18] or contact-separation mode [19–22]. Especially, the

sliding mode is widely used in harvesting rotational energy and has the advantage of generating high electric output [17]. However, in the sliding mode-based TENGs, the relative displacement between two contacting triboelectric layers may cause severe abrasion, which lowers the output power and shortens the service life of the devices [23]. However, on the other hand, compared to the contact-separation mode, the sliding mode with grids electrode typically can generate electric output with higher frequency, which is desired for practical applications [24–27]. Therefore, to reduce the abrasion when harvesting rotational energy, increase the durability of the TENG devices, and, in the meantime, improve the frequency of the electric output remain challenging.

To address this issue, we propose a cam and a movable frame-based triboelectric nanogenerator (CMF-TENG) that can be used to harvest energy from the rotational motion (e.g., triggered by ambient mechanical energy). The movable frame can move linearly driven by the rotation of the cam. The linear movement of the movable frame can then lead to the contact separation of the triboelectric layers within each subunit periodically, thus generates electric output. With our specific design of the cam (will be discussed later), the frequency of the electric signals from each subunit can be raised. For example, when the simulated rotating movement reaches 60 rpm (i.e., 1 Hz), the electric output from each subunit can achieve a frequency of 3 Hz. The designed CMF-TENG has 6 sub-triboelectrification units. Each subunit can deliver an average electric output of around 200 V of open-circuit voltage, 2.9 μA of short-circuit current, and 96 nC of transferred charge when the triggered rotational speed was at 60 rpm.

With the assistance of a rectifying circuit, the CMF-TENG can light up 113 blue light-emitting diodes (LEDs) (connected in series) when the wind speed was at 13.9 m/s. With the assistance of a rectifying circuit and a commercial capacitor, the CMF-TENG can also power a commercial electronic thermometer when the wind speed was at the same condition. By using our novel design, there is only contact-separation between the triboelectric layers, without in-plane relative sliding between the triboelectric layers. Therefore, the abrasion between such layers is expected to be minimal, resulting in high durability of our device. The CMF-TENG can work continuously for at least 8 h without decreasing in electric output. This structure technically allows adding additional subunit to improve the electric output of the entire device. In short, we propose a novel mechanical design of triboelectric nanogenerator with great durability and stability that can harvest energy from the ambient environment and achieve self-powered sensing.

2. Results and discussion

2.1. Structure and working principle of CMF-TENG

As can be seen from Fig. 1a and d, the CMF-TENG consisted of an outside box, a cam, a movable frame, along with 6 sub-triboelectrification units. For each unit, a layer of copper served as both triboelectric layer and electrode; and a layer of polytetrafluoroethylene (PTFE), which served as another triboelectric layer, was placed on top of another copper layer, serving as the other electrode layer (Fig. 1b). Fig. 1c shows an enlarged illustration of the supporting plate. The PTFE and the electrode (i.e., copper) layer were attached to the supporting plate. The hole in the middle of the plate is designed for the movement of the column of the movable frame. Fig. 1f shows the picture of an acrylic movable frame plus four plates that will be fixed on the platform (described in Figure S1). The layer of copper served as both triboelectric layer and electrode were attached to the side of the movable frame, and sponges were installed underneath each of the layer of copper to increase contact between the friction layers. Electrical wires were connected to each electrode layer for characterizing the electric output. (Additional information on the design of the cam and the CMF-TENG is described in the experimental section and supporting information.)

Fig. 1e displays the designed cam. The idea of introducing the cam is to transform rotary motion triggered by environmental mechanical movement (e.g., wind) into linear motions. With the aid of the movable frame, the design can then lead to the contact and separation of two different triboelectric layers (i.e., copper and PTFE) in each unit periodically. Through those contact and separation events, the mechanical energy can be converted into electric output (more energy harvesting mechanisms will be discussed in the later section). In this structure, the cam is used to drive the movable frame moving linearly. Therefore, the design of cam is a key to achieve better performance. Using in this design, when the number of noses of the cam is even, the distance between the sides of the cam will mostly be the same, the frame (i.e., the follower) may not move linearly when the cam rotates in our design. Among the cam with odd numbers of noses, it can be expected that the cam with one nose can only covert rotary motions into linear motions without increasing the frequency of the electric output. The cam with five or more noses would limit the strokes (i.e., moving distance) of the movable frame, which may result in the reduction of the electric output, or may require additional space to move effectively. Therefore, we chose the cam with three noses as the optimal design. (Additional information on cam design is described in the experimental section and supporting information.) It is worth noting that the entire CMF-TENG could be further enclosed completely by proper packaging, implying that it may be capable of harvesting environmental energy under harsh
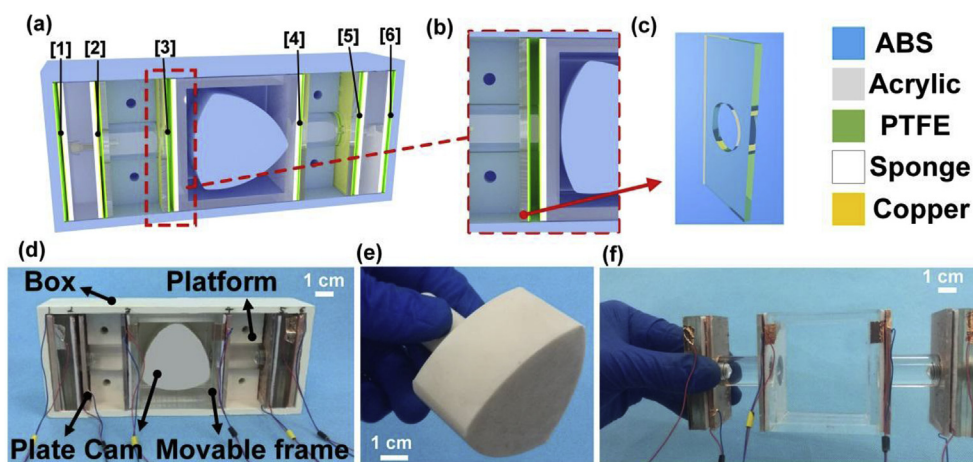
Fig. 1. Structural design of the CMF-TENG. (a) Schematic diagram showing the structural design of the CMF-TENG. (b) Enlarged illustration reveals the multilayered structure. (c) An illustration of the support plate. (d) Photograph of the as-fabricated CMF-TENG (scale bar, 1 cm). (e) Photograph of the designed cam (scale bar, 1 cm). (f) Photograph of an acrylic material-based movable frame plus four plates that will be fixed on the platform (scale bar, 1 cm).
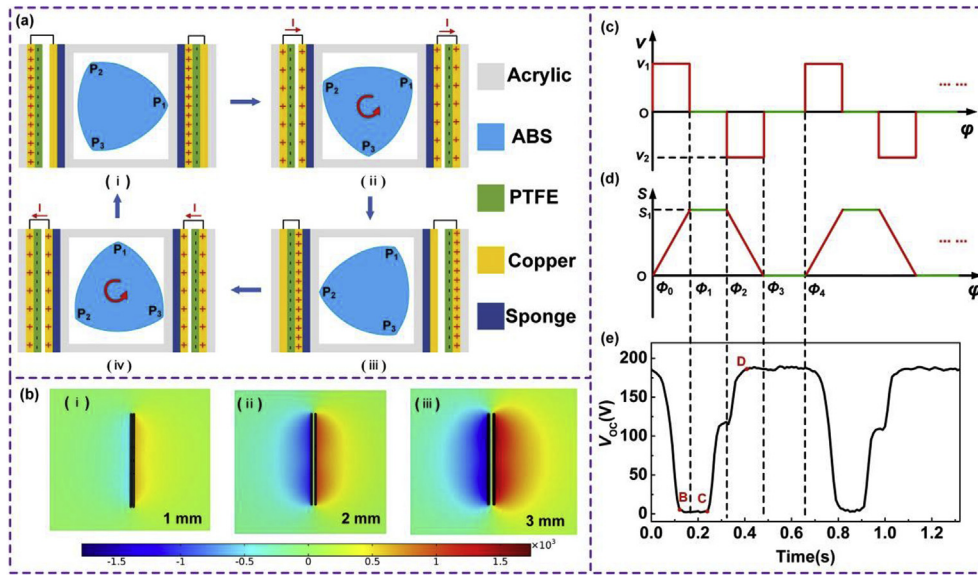
Fig. 2. Schematics of the operating principle of the cam and movable frame-based triboelectric nanogenerator (CMF-TENG). (a) A full cycle of the electricity generation processes using two units of the CMF-TENG. (b) Potential distribution results using COMSOL is employed to elucidate the working principle of the CMF-TENG. The relationships between the velocity (v) (c) and the displacement (S) (d) of the follower with the angle (φ) of rotation of the cam. (e) Two cycles of the open-circuit voltage (V_{OC}) signal from one sub-triboelectrification unit (#4) located on the right side of the CMF-TENG.

environmental conditions. The detailed fabrication procedures of CMF-TENG are described in the experimental section and supporting information.

As the rotary motion triggered by environmental mechanical movement appears, the cam rotates, as shown in Fig. 2a. Firstly, we focus on the sub-triboelectrification unit on the right side of the cam. At the initial state, in Fig. 2a i, the two triboelectric layers (i.e., copper and PTFE) are forced to be in contact with each other. Owing to contact-electrification, positively triboelectric charges appear on the copper layer and negative charges are on the PTFE layer, according to triboelectric series [28]. As the cam rotates, e.g., counterclockwise, it forces the movable frame to move from right to left, which results in the two triboelectric layers in the right sub-triboelectrification unit separating (Fig. 2a ii). As the separation distance increases, the electrons move from the copper layer underneath the PTFE to the other copper layer (on the left side of the same subunit) through external electrical wires to balance the build-up electric field, resulting in electric output. The simulation results using COMSOL also show that the potential difference between two triboelectric layers increases as the separating distance raises, showing in Fig. 2b.

While the separation distance (of the two triboelectric layers) of the right subunit reaches its maximum, the two triboelectric layers on the left subunit are in contact with each other (Fig. 2a iii). As the cam keeps rotating, the two triboelectric layers in the right subunit become closer, which results in the electrons flow from the copper on the left to the copper on the right (i.e., underneath the PTFE layer), until the two triboelectric layers are in contact with each other (Fig. 2a i) to complete a full cycle. These can then repeatedly convert the mechanical movement to electric output. The rotating of the cam also leads to the linear motion between triboelectrification layers within other subunits, for example, the triboelectric layers within unit 1, 3 and 5 are contacted and separated simultaneously as they located on the left side of the cam; while the layers in unit 2, 4 and 6 are operating simultaneously as they appear on the right side of the cam. A slow-motion animation of the operation was added as supporting movie S1 to help understand the motion processes of the CMF-TENG. The electric output can then be generated by the mechanisms mentioned above.

Supplementary data related to this article can be found at https://doi.org/10.1016/j.nanoen.2019.03.019.

The pressure angle is the angle between the direction of force (F) from the cam and the direction of velocity (v) of the follower without considering the friction. The smaller the pressure angle of the follower can lead to the greater the force along the velocity direction. When the

pressure angle is too large, the force transmission performance will be deteriorated [29]. In this structure, since the cam contacts with the inner surface of the movable frame, which can be considered as a flat-face follower (as shown in Figure S2), the pressure angle is zero.

ϕ is the angle of the cam at each moment. We use ϕ_0 to ϕ_4 to further illustrate the motion between the cam and the movable frame. As shown in Figure S2, when the angle of the cam is at ϕ_0, the cam contacts the movable frame and the actuating travel of the follower (i.e., movable frame) starts. Define the position of the moving frame at this angle as 0, as shown in Fig. 2d. When the angle of the cam is at ϕ_1, it is the end of the actuating travel of the movable frame. The displacement of the movable frame during this actuating travel period is S_1. According to the general expression of the law of polynomial motion [30], the relationship between the displacement (S) and velocity (v) with the angle (φ) of the cam is:

$$S = \frac{S_1}{\phi_1} \varphi \quad (\phi_0 < \varphi > \phi_1) \tag{1}$$

$$v = \frac{S_1 \omega}{\phi_1} \quad (\phi_0 < \varphi > \phi_1) \tag{2}$$

where $d\varphi/dt = \omega$ is the angular velocity of the cam. When the angle of the cam rotated from ϕ_1 to ϕ_2, the movable frame does not move because the cam and the movable frame do not touch. When the angle of the cam rotated from ϕ_2 to ϕ_3, the other cam nose drives the movable frame to move in the opposite direction (left). Since the angle of each cam nose is same, we could infer that

$$\phi_1 = \phi_3 - \phi_2 \tag{3}$$

The equation of actuating travel of the reverse push (i.e., the movable cam move to origin) can then be written as:

$$S = \frac{\phi_1 + \phi_2}{\phi_1} S_1 - \frac{S_1 \varphi}{\phi_1} \quad (\phi_2 < \varphi > \phi_3) \tag{4}$$

$$v = -\frac{S_1 \omega}{\phi_1} \quad (\phi_2 < \varphi > \phi_3) \tag{5}$$

When the angle of the cam rotated from ϕ_3 to ϕ_4, the movable frame does not move, and the relative position of the cam and the movable frame is the same as ϕ_0 (more calculation process will be discussed in the support information).

Fig. 2c and d show the relationship between the velocity (v) and the displacement (S) of the follower with the angle (φ) of rotation of the cam. Fig. 2e shows two cycles of the open-circuit voltage (V_{OC}) signals

from the sub-triboelectrification unit 4 within the CMF-TENG at 30 rpm. It can be seen from the comparison between Fig. 2d and e that the experimentally measured voltage signals have a good correspondence with the theoretical inference. We use the electric signals from the subunit #4, which is located on the right side of the cam, as an example. The cam starts from ϕ_0 to drive the movable frame to the right, and the open-circuit voltage gradually decreases. Since the displacement of the movable frame is slightly greater than the separation distance of the two triboelectric layers (by design), it can result in better contact (or increasing the contact area) between two such layers. As a result, at B point in Fig. 2e, two triboelectric layers are already in full contact. As the cam keeps rotating, at point C, the cam nose P_1 is now completely separated from the follower (i.e., movable frame). In the meantime, the movable frame moves to the left by a small distance due to the elastic force from the sponge layer. This may be one of the possible explanations of the shoulder between C and D in Fig. 2e. As the cam keeps rotating counterclockwise, the movable frame then is driven to the left by the cam nose P_2 (at angle ϕ_2, see Figure S2). At the D point, in Fig. 2e, the open-circuit voltage from subunit #4 reaches its maximum (i.e., the separation distance between the two triboelectrification layers reaches maximum). Since the movable frame does not move when the angle is from ϕ_3 to ϕ_4 (or ϕ_0), the electric signal does not change during this period. As the cam keeps rotating, the movable frame then continuously moves to the next cycle.

2.2. Performance of CMF-TENG

To characterize the electrical performance of the CMF-TENG, we firstly use an electric motor to provide rotating movements. The rotating movement can then be transformed into linear motion, owing to the designed cam, thus resulting in the abovementioned motion of the CMF-TENG. Fig. 3a–c shows the electric output, including open-circuit voltage (V_{OC}), short-circuit current (I_{SC}), and transferred charges (Q_{SC}), of each sub-triboelectrification unit using the electric motor operating at 60 rpm. As can be seen from the figures, as the triggered rotating movement performs at 60 rpm (i.e. 1 Hz), the frequency of the electric output is measured at 3 Hz (e.g., six electric output peaks in 2 s). The results suggest that the designed cam can increase the frequency of the electric output. It is worth noting that all the PTFE layers were pre-treated by electron injection before installing into the subunits, following the procedure describe previously with a slight modification [31]. The experimental setup of the electron injection is displayed in Figure S3d and the detailed treating procedures are described in the experimental section. As can be seen from Figure S3a, the voltage output (V_{OC}) of the CMF-TENG increased by 40% after the electron injection treatment. The output enhancement can also be observed in

I_{SC} and Q_{SC}, Figure S3b-c. Therefore, all the experimental results present in the following sections are using the pre-treated PTFE for output enhancement.

When two subunits were connected in parallel, the V_{OC} increased from around 200 V (one unit) to around 277 V. Similar enhancement can be found when three subunits were connected in parallel (Fig. 3d and S4a). Fig. 3e–f and Figure S4b-c show a similar increase in the I_{SC} and Q_{SC}. Interestingly, when two subunits were connected in series, the V_{OC}, $I_{SC,}$ and Q_{SC} only increased slightly (or were almost the same as the output of one subunit), compared to the parallel connections. Similar results can be observed as three subunits were connected in series (Figure S5). One possible explanation is that as the different subunits are connected in series, the charge induced by the PTFE on one copper (on one unit) may partially cancel out the charge induced on another connected copper layer on the other subunit, thus, leading to lower overall electric output (compared to the parallel connections). The results suggest that connecting each subunit in parallel could result in higher electric output in our case. As the previous study also suggested that the power management of the TENG still has plenty of room for improvement, more works could be done in the future in this direction [10,32].

The output performance of the CMF-TENG at different triggered rotational speed was also investigated. Various rotational speeds can be transformed into different operation frequencies of CMF-TENG. For example, higher rotational speed leads to higher operating frequencies, and vice versa. Fig. 4 a and c demonstrate that the V_{OC} and Q_{SC} were almost independent to operation frequencies. However, the I_{SC} increased as frequency raised. The potential explanation is that as the transferred charges (Q_{SC}) remain almost constant at different operating frequencies, whereas the contact time between the two triboelectric layers in each subunit changed at different operating frequencies, thus, the I_{SC} changes. For instance, the flow rate of charges can become higher at higher operating frequency, which can possibly lead to a higher current output. The results are also consistent with previous studies [33].

For better understand the output performance when external loads are applied, the voltage and current output at different resistive loads (R) were also measured. As can be seen from Fig. 4d, as the resistance was low, which is similar to a short-circuit scenario, the voltage output of the CMF-TENG was low, but the current output was high. However, as the resistance increased, the voltage output increased but the current decreased. The voltage reached the maximum at highest applied resistance (2,000 MΩ), which is similar to an open-circuit situation, whereas the current became minimum. The power output (P) of the CMF-TENG can then be calculated as $P = I^2 R$ and the maximum power output of the CMF-TENG can be achieved at a matched impedance of
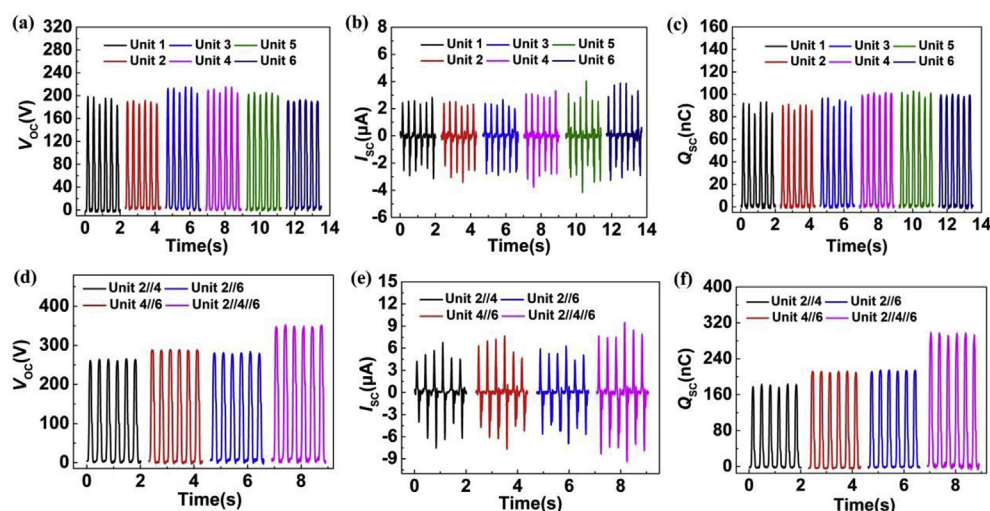

Fig. 3. Electric output performance of the cam and movable frame-based triboelectric nanogenerator (CMF-TENG) at a triggered rotation speed operated at 60 rpm. Open-circuit voltage (V_{OC}) (a), short-circuit current (I_{SC}) (b), and transferred charges (Q_{SC}) (c) of each sub-triboelectrification unit within the CMF-TENG. V_{OC} (d), I_{SC} (e), and Q_{SC} (f) of two or three subunits (unit 2, 4, and/or 6) connected in parallel.
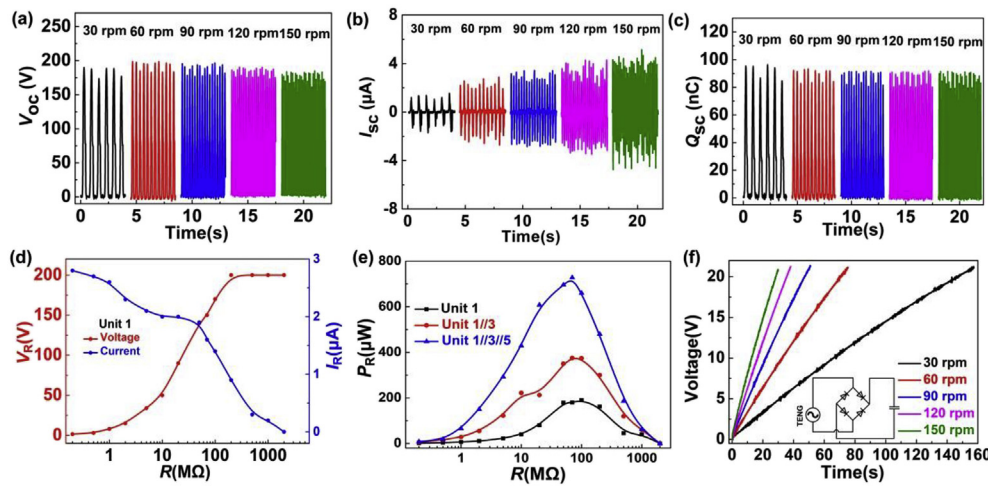
Fig. 4. Electric output performance of the cam and movable frame-based triboelectric nanogenerator (CMF-TENG) with one subunit working when triggered rotational speed is at 60 rpm. Open-circuit voltage (V_{OC}) (a), short-circuit current (I_{SC}) (b), and transfer-charge (Q_{SC}) (c) of CMF-TENG for one subunit working at various rotating speeds. (d) The voltage and current output of one subunit of CMF-TENG at different external loads. (e) The instantaneous power of 1–3 subunits at different external loads. (f) Voltage of a commercial capacitor (10 μF) charging by six subunits connected in parallel under various triggered rotating speeds.

around 70 MΩ, Fig. 4e. As can be seen from Fig. 4e, the power output increase from 180 μW (1 subunit) to around 728 μW, when three subunits were connected in parallel. Fig. 4f demonstrates that the CMF-TENG can charge a commercial 10 μF capacitor to 20 V in minutes, depending on the rotating speed. The CMF-TENG was first connected to a rectifying circuit (inset of Fig. 4f) and then be used to charge the capacitor. As can be seen from Fig. 4f, a higher rotational speed can lead to a faster charging time.

2.3. Demonstration

CMF-TENG was connected to a fan blade for the demonstration of wind energy harvesting, see Fig. 5a. A controlled wind source was flowed by the fan blade for these demonstrations. As can be seen from Fig. 5b and supporting Video S2, the CMF-TENG can light up 113 blue LEDs (connected in series) with the assistance of a rectifying circuit (wind speed: 13.9 m/s). In another practical application, the CMF-TENG was connected to a rectifying circuit first and then to a commercial capacitor (330 μF) to power a commercial electronic thermometer when the wind speed was at 13.9 m/s (see Fig. 5c and the supporting Video S3). The results imply that the CMF-TENG can not only be used to harvest energy from the ambient environment, but also can achieve self-powered sensing. The durability of the CMF-TENG was also

evaluated by continuously operating it for about 8 h at 60 rpm. Fig. 5d displays that the electric output remains almost constant after continuous operation for about 8 h (i.e., about 86,400 contact-separation events between the triboelectric layers), suggesting the excellent robustness of the CMF-TENG.

Supplementary data related to this article can be found at https://doi.org/10.1016/j.nanoen.2019.03.019.

3. Conclusions

We proposed a novel triboelectric nanogenerator that achieves energy harvesting through a combination of a cam and a movable frame. The movement of the movable frame was driven by the rotary motion of the cam triggered by environmental mechanical or simulated rotational movement. There are 6 sub-triboelectrification units in the CMF-TENG. When the movable frame moves linearly (left and right), the contact-separation of the triboelectric layers within each subunit can be achieved, thus resulting in electric output. The design structure can technically allow more subunits to be added to achieve higher electric output. The maximum power output of the CMF-TENG can be reached at a matched impedance of around 70 MΩ, and the power output increased from 180 μW (1 subunit) to around 728 μW when three subunits were connected in parallel. The CMF-TENG also can light up 113
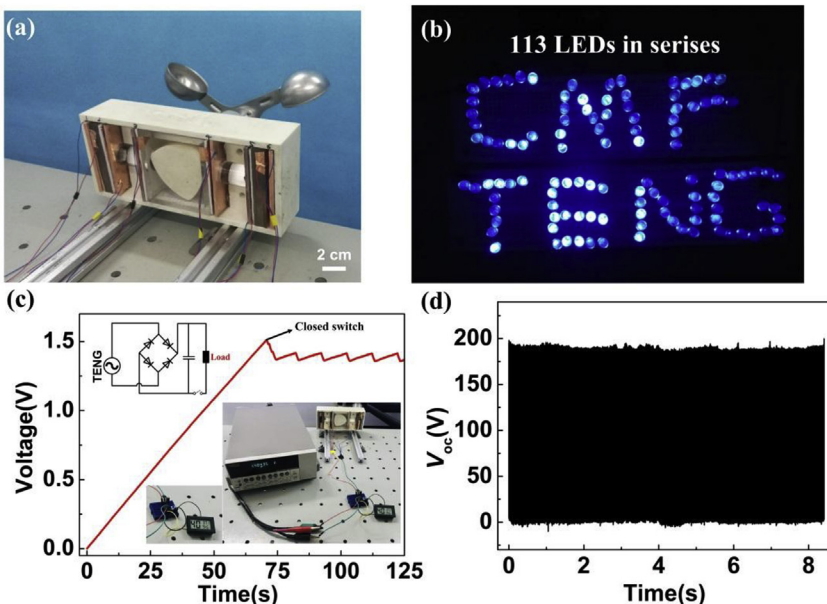

Fig. 5. Wind energy harvesting by the cam and movable frame-based triboelectric nanogenerator (CMF-TENG). (a) Photograph of the as fabricated CMF-TENG for harvesting wind energy (scale bar, 2 cm). (b) The CMF-TENG lights up 113 blue LEDs (connected in series) at a wind speed of 13.9 m/s. (c) The CMF-TENG powers the thermometer at a wind speed of 13.9 m/s. (d) Stability and durability test of the CMF-TENG for about 8 h.

LEDs at the wind speeds of 13.9 m/s, with the assistance of a rectifying circuit. The CMF-TENG can also power a commercial thermometer at the same wind speed with the assistance of a commercial capacitor and a rectifying circuit. This demonstrates the capability of using CMF-TENG to power electronic devices in our daily life. The experimental results also show that the voltage output remained almost consistent throughout the roughly 8 h testing time, which suggests the robustness of CMF-TENG in practical applications.

4. Experimental section

4.1. Fabrication of the CMF-TENG

The designed CMF-TENG consisted of an outside box, a cam, plates, and a movable frame. Firstly, the box, 186 (length) × 80 (height) × 43 (thick), and the cam with a camshaft were made of acrylonitrile buta-diene styrene (ABS) by a milling machine. One bearing was installed on the box. The cam was then installed on the box through camshaft that fits the bearing and the camshaft was connected to the electric motor or fan blade. The movable frame was then placed surrounding the cam in the box. Taking advantage of this design, the movable frame can move linearly through the rotation of the cam. Acrylic plates with the dimension of 69 (length) × 35 (wide) × 3 (thick) mm and a 10 mm in diameter circle in the middle were prepared by a laser cutting machine. There are 6 sub-triboelectric units in the designed CMF-TENG. As shown in Figure S1, one side of the acrylic plate was pasted on the platforms by a 3 M glue to serve as a support for the frame. Prior to that, one copper layer, which serves as an electrode layer, was attached to each of the acrylic plates, followed by attaching a layer of PTFE on top of each copper layer. These PTFE layers served as one of two tribo-electric layers for the subunits #2, 3, 4 and 5. For subunits #1 and 6, a PTFE layer (with a copper layer underneath) was placed on the left and right inner wall of the box, Figure S1a. In addition to the PTFE layers, six layers of copper, which served as the other triboelectric layer in each subunit, with a sponge layer underneath, were attached on two sides of the frame (for 2 subunits, #3 and #4), and two sides of the two blocks (for 4 subunits, #1, 2, 5, and 6) that were connected to the column, Figure S1c. Therefore, for each subunit, there are 2 tribo-electric layers, PTFE (with a layer of copper underneath as an electrode) and copper (with a layer of sponge underneath to improve the contact). Additional descriptions can be found in the supporting information.

4.2. Electron injection on PTFE film

The electron injection on the PTFE film was achieved by a high voltage power source (ET2673A, Nanjing Entai Electronic Instruments Plant), as shown in Figure S3d. Firstly, the pin electrodes were connected in series and then to the cathode of the power source. Then, PTFE was placed under the pin electrodes with a vertical distance of 3 cm. The power source was then operated at 7 kV for 5 min for electron injection.

4.3. Electrical measurement

A two-phase Hybrid Step-servo Motor (J-5718HBS401, Yisheng, China) was connected to the camshaft of the cam through a coupling for conducting the experiments at different rotational speeds. Wind speed alarm instrument (NJLS-TJFS, Longshun, China) was used to measure the reported wind speeds. The output wires from the CMF-TENG was connected to an electrometer (6514, Keithley, USA), which connected to a data acquisition system (PCI-6259, National Instruments, USA) and a computer. A programmed Labview code was used to collect the electric output signal.

Appendix A. Supplementary data

Conflicts of interest

The authors declare no conflict of interest.

References

[1] M. Höök, X.T.J.E. Policy, Energy Policy 52 (2013) 797–809.
[2] M. A, T. M, Renew. Sustain. Energy Rev. 11 (2007) 1388–1413.
[3] Z.L. Wang, J. Song, Science 312 (2006) 242.
[4] S.P. Beeby, R.N. Torah, M.J. Tudor, P. Glynne-Jones, T.O. Donnell, C.R. Saha, S. Roy, J. Micromech. Microeng. 17 (2007) 1257.
[5] K. Dong, J. Deng, Y. Zi, Y.-C. Wang, C. Xu, H. Zou, W. Ding, Y. Dai, B. Gu, B. Sun, Z.L. Wang, Adv. Mater. 29 (2017) 1702648.
[6] K. Dong, Y.-C. Wang, J. Deng, Y. Dai, S.L. Zhang, H. Zou, B. Gu, B. Sun, Z.L. Wang, ACS Nano 11 (2017) 9490–9499.
[7] M. Xu, P. Wang, Y.-C. Wang, S.L. Zhang, A.C. Wang, C. Zhang, Z. Wang, X. Pan, Z.L. Wang, Adv. Energy Mater. 8 (2017) 1702432.
[8] S.L. Zhang, M. Xu, C. Zhang, Y.-C. Wang, H. Zou, X. He, Z. Wang, Z.L. Wang, Nanomater. Energy 48 (2018) 421–429.
[9] R. Liu, X. Kuang, J. Deng, Y.-C. Wang, A.C. Wang, W. Ding, Y.-C. Lai, J. Chen, P. Wang, Z. Lin, H.J. Qi, B. Sun, Z.L. Wang, Adv. Mater. 30 (2018) 1705195.
[10] Z.L. Wang, Mater. Today 20 (2017) 74–82.
[11] A. Nivedita, L.Z. Steven, S. Fereshteh, O. Diego, W. Yi-Cheng, G. Mohit, W. Zhengjun, S. Thad, W. Zhong Lin, D.A. Gregory, Proc. ACM Interact. Mob. Wearable Ubiquitous Technol. 2 (2018) Article Number:60.
[12] Y. Chen, Y.-C. Wang, Y. Zhang, H. Zou, Z. Lin, G. Zhang, C. Zou, Z.L. Wang, Adv. Energy Mater. 0 (2018) 1802159.
[13] C. Xu, Y. Zi, A.C. Wang, H. Zou, Y. Dai, X. He, P. Wang, Y.-C. Wang, P. Feng, D. Li, Z.L. Wang, Adv. Mater. 30 (2018) 1706790.
[14] Y. Zi, H. Guo, Z. Wen, M.-H. Yeh, C. Hu, Z.L. Wang, ACS Nano 10 (2016) 4797–4805.
[15] H. Guo, J. Chen, M.H. Yeh, X. Fan, Z. Wen, Z. Li, C. Hu, Z.L.J.A.N. Wang, ACS Nano 9 (2015) 5577–5584.
[16] S. Niu, Y. Liu, S. Wang, L. Lin, Y.S. Zhou, Y. Hu, Z.L.J.A.M. Wang, Adv. Mater. 25 (2013) 6184–6193.
[17] Q. Tang, M.H. Yeh, G. Liu, S. Li, J. Chen, Y. Bai, L. Feng, M. Lai, K.C. Ho, H.J.N.E. Guo, Nanomater. Energy 47 (2018) 74–80.
[18] G. Zhu, J. Chen, Y. Liu, P. Bai, Y.S. Zhou, Q. Jing, C. Pan, Z.L.J.N.L. Wang, Nano Lett. 13 (2013) 2282–2289.
[19] J. Chen, J. Yang, H. Guo, Z. Li, L. Zheng, Y. Su, Z. Wen, X. Fan, Z.L.J.A.N. Wang, ACS Nano 9 (2015) 12334–12343.
[20] B. Peng, Z. Guang, L. Zong-Hong, J. Qingshen, Z. Gong, M. Jusheng, W.J.A.N. Zhong Lin, ACS Nano 7 (2013) 3713–3719.
[21] J. Qian, X. Wu, D.S. Kima, D.W.J.S. Lee, A.A. Physical, Sensor Actuator Phys. 263 (2017) 600–609.
[22] Y. Weiqing, Z. Guang, Y. Jin, B. Peng, S. Yuanjie, J. Qingsheng, C. Xia, W.J.A.N. Zhong Lin, ACS Nano 7 (2013) 11317–11324.
[23] M.L. Seol, J.W. Han, D.I. Moon, K.J. Yoon, C.S. Hwang, M.J.N.E. Meyyappan, Nanomater. Energy 44 (2018) 82–88.
[24] Y. Lee, W. Kim, D. Bhatia, H.J. Hwang, S. Lee, D.J.N.E. Choi, Nanomater. Energy 38 (2017) 326–334.
[25] G. Liu, R. Liu, H. Guo, Y. Xi, D. Wei, C.J.A.E.M. Hu, Adv. Electron. Mater. 2 (2016) 1500448.
[26] I.W. Tcho, S.B. Jeon, S.J. Park, W.G. Kim, I.K. Jin, J.K. Han, D. Kim, Y.K.J.N.E. Choi, Nanomater. Energy 50 (2018) 489–496.
[27] W. Kim, H.J. Hwang, D. Bhatia, Y. Lee, J.M. Baik, D.J.N.E. Choi, Nanomater. Energy 21 (2016) 19–25.
[28] D.K. Davies, J. Phys. D Appl. Phys. 2 (1969) 1533.
[29] P. Flores, R. Leine, C. Glocker, Nonlinear Dynam. 69 (2012) 2117–2133.
[30] P. Mermelstein, M. Acar, Eng. Comput. 19 (2004) 241–254.
[31] L.M. Zhang, C.B. Han, T. Jiang, T. Zhou, X.H. Li, C. Zhang, Z.L. Wang, Nanomater. Energy 22 (2016) 87–94.
[32] H. Qin, G. Cheng, Y. Zi, G. Gu, B. Zhang, W. Shang, F. Yang, J. Yang, Z. Du, Z.L. Wang, Adv. Funct. Mater. 0 (2018) 1805216.
[33] Z. Lin, Q. He, Y. Xiao, T. Zhu, J. Yang, C. Sun, Z. Zhou, H. Zhang, Z. Shen, J. Yang, Z.L. Wang, Adv. Mater. Technol. 3 (2018) 1800144.

Tinghai Cheng received the B.S., M.S. and Ph.D. degrees from Harbin Institute of Technology in 2006, 2008 and 2013, respectively. He was a visiting scholar in School of Materials Science and Engineering at Georgia Institute of Technology under the supervision of Prof. Zhong Lin (Z. L.) Wang from 2017 to 2018. Currently, he is an associate professor in the school of mechatronic engineering, Changchun University of Technology. His research interests are triboelectric nanogenerators, piezoelectric energy harvester, and piezoelectric actuators.

Qi Gao was born in 1995 Jilin province, majored in mechanical engineering and achieved the B.E. degree from Changchun University of Technology in 2017. He continues pursuing a Master of Engineering degree in the same school. His research interests are triboelectric nanogenerator.

Yikang Li was born in 1994 Jilin province, majored in mechanical engineering and achieved the B.E. degree from Changchun University of Technology in 2017. He continues pursuing a Master of Engineering degree in the same school. His research interests are triboelectric nanogenerator.
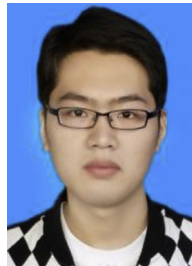
Teng Ma was born in Shandong province, China, in 1992. He received the BS degree in thermal energy and power engineering from the Dezhou University, Shandong, China, in 2016. He continued pursuing a Master of Engineering degree from Changchun University of Technology, Changchun, China, in 2017. His research interests include piezoelectric generator and triboelectric nanogenerator.

Dr. Yi-Cheng Wang is an Assistant Professor in the Department of Food Science and Human Nutrition at the University of Illinois at Urbana-Champaign. His research interests include the synthesis of advanced materials for sensors and food-safety applications. He received a B.S. in Bio-Industrial Mechatronics Engineering from National Taiwan University, his M.S. in Chemistry and Ph.D. in Biological Systems Engineering from the University of Wisconsin-Madison, and completed his postdoctoral training at the Georgia Institute of Technology. Among other awards and honors, he has received the Institute of Food Technologists' Feeding Tomorrow Graduate Scholarship and a Wisconsin Distinguished Graduate Fellowship.

Prof. Zhong Lin (Z. L.) Wang is the Hightower Chair in Materials Science and Engineering and Regents' Professor at Georgia Tech, the chief scientist and director of the Beijing Institute of Nanoenergy and Nanosystems, Chinese Academy of Sciences. His discovery and breakthroughs in developing nanogenerators and self-powered nanosystems establish the principle and technological road map for harvesting mechanical energy from environmental and biological systems for powering personal electronics and future sensor networks. He coined and pioneered the field of piezotronics and piezophototronics.